

RESEARCH ARTICLE

# Spatial neuronal synchronization and the waveform of oscillations: Implications for EEG and MEG

Natalie Schaworonkow<sup>1,2</sup>, Vadim V. Nikulin<sup>3,4,5,6\*</sup>

**1** Frankfurt Institute for Advanced Studies, Johann Wolfgang Goethe University, Frankfurt am Main, Germany, **2** Department of Neurology & Stroke, and Hertie Institute for Clinical Brain Research, University of Tübingen, Tübingen, Germany, **3** Department of Neurology, Max Planck Institute for Human Cognitive and Brain Sciences, Leipzig, Germany, **4** Centre for Cognition and Decision Making, National Research University Higher School of Economics, Moscow, Russian Federation, **5** Neurophysics Group, Department of Neurology, Charité-University Medicine Berlin – Campus Benjamin Franklin, Berlin, Germany, **6** Bernstein Center for Computational Neuroscience Berlin, Berlin, Germany

\* [nikulin@cbs.mpg.de](mailto:nikulin@cbs.mpg.de)



**OPEN ACCESS**

**Citation:** Schaworonkow N, Nikulin VV (2019) Spatial neuronal synchronization and the waveform of oscillations: Implications for EEG and MEG. *PLoS Comput Biol* 15(5): e1007055. <https://doi.org/10.1371/journal.pcbi.1007055>

**Editor:** Francesco P. Battaglia, Radboud Universiteit Nijmegen, NETHERLANDS

**Received:** September 11, 2018

**Accepted:** April 26, 2019

**Published:** May 14, 2019

**Copyright:** © 2019 Schaworonkow, Nikulin. This is an open access article distributed under the terms of the [Creative Commons Attribution License](https://creativecommons.org/licenses/by/4.0/), which permits unrestricted use, distribution, and reproduction in any medium, provided the original author and source are credited.

**Data Availability Statement:** The EEG data were previously collected as part of the "Leipzig Cohort for Mind-Body-Emotion Interactions" data set (LEMON). The data underlying the results are available from: [http://fcon\\_1000.projects.nitrc.org/indi/retro/MPI\\_LEMON.html](http://fcon_1000.projects.nitrc.org/indi/retro/MPI_LEMON.html).

**Funding:** NS acknowledges support through a EXIST Transfer of Research Grant from the German Federal Ministry for Economic Affairs and Energy and from the Quandt foundation. VVN acknowledges support by the HSE Basic Research Program and the Russian Academic Excellence

## Abstract

Neuronal oscillations are ubiquitous in the human brain and are implicated in virtually all brain functions. Although they can be described by a prominent peak in the power spectrum, their waveform is not necessarily sinusoidal and shows rather complex morphology. Both frequency and temporal descriptions of such non-sinusoidal neuronal oscillations can be utilized. However, in non-invasive EEG/MEG recordings the waveform of oscillations often takes a sinusoidal shape which in turn leads to a rather oversimplified view on oscillatory processes. In this study, we show in simulations how spatial synchronization can mask non-sinusoidal features of the underlying rhythmic neuronal processes. Consequently, the degree of non-sinusoidality can serve as a measure of spatial synchronization. To confirm this empirically, we show that a mixture of EEG components is indeed associated with more sinusoidal oscillations compared to the waveform of oscillations in each constituent component. Using simulations, we also show that the spatial mixing of the non-sinusoidal neuronal signals strongly affects the amplitude ratio of the spectral harmonics constituting the waveform. Finally, our simulations show how spatial mixing can affect the strength and even the direction of the amplitude coupling between constituent neuronal harmonics at different frequencies. Validating these simulations, we also demonstrate these effects in real EEG recordings. Our findings have far reaching implications for the neurophysiological interpretation of spectral profiles, cross-frequency interactions, as well as for the unequivocal determination of oscillatory phase.

## Author summary

The electrical activity in the human brain demonstrates oscillations of intricate complexity. Interestingly, such complex waveforms are primarily visible in invasive recordings but not so much when neuronal activity is recorded with non-invasive methods such as

Project "5-100". The funders had no role in study design, data collection and analysis, decision to publish, or preparation of the manuscript.

**Competing interests:** The authors have declared that no competing interests exist.

electroencephalography. Yet a specific waveform is informative about the postsynaptic processes which are at the core of our understanding of cortical excitability and information transfer in neuronal networks. In our study, we show with simulations and real EEG data, how temporal delays between different cortical sources can contribute to a more sinusoidal or non-sinusoidal shape of neuronal oscillations. We illustrate how, depending on the temporal delays, low- and high-frequency components of oscillations can be enhanced or attenuated to a different degree thus affecting the shape of oscillations and corresponding spectra which are often associated with specific functional consequences. We further show how this phenomenon can challenge our understanding of the link between neuronal oscillations and motor function, cognition and perception.

## Introduction

Neuronal oscillations are ubiquitous in the human brain, being present in both cortical and subcortical structures. Moreover, they have been shown to be relevant for sensory [1, 2], motor [3, 4] and cognitive [5, 6] functions. Traditionally, neuronal oscillations as recorded by EEG/MEG are considered to be sinusoidal. This observation is particularly driven by the analysis tools frequently used in neuroscience. These often include Fourier, Morlet wavelet and Gabor transforms, all of which use sinusoids as a basis function [7]. There is no a-priori reason why exactly these basis functions would be most relevant for describing neuronal oscillations ("Fourier fallacy" [8]). Many nonlinear periodic processes in nature are in fact quasi-sinusoidal [9]. For instance, the non-sinusoidal nature of ocean waves has for long time been recognized [10], where it was emphasized that conventional spectral analysis is not sensitive to the non-sinusoidal nature of periodic processes. Due to the complexity of such waves, analysis in time domain is often suggested and elaborate measures of horizontal and vertical asymmetries have been presented [11]. A similar claim has been recently voiced for large scale neuronal oscillations [12], which represent a particularly good example where many nonlinearities are present including thresholds, exponential decays and non-linear coupling between neuronal elements. It is therefore not surprising that often neuronal recordings only approximately resemble sinusoidal processes especially when they are obtained with invasive techniques [13, 14]. This in turn indicates that other concepts and analysis tools are needed for a more adequate description of periodic neuronal processes recorded with EEG/MEG.

Waveform was largely neglected in large scale EEG/MEG analysis up until recently [15, 16]. However, the reasons why non-invasive neuronal recordings rather show sinusoidal oscillations in contrast to invasive recordings have not yet been clearly identified. Some evidence for non-sinusoidality is also visible in the spectral domain, as non-sinusoidal processes are manifested through the presence of additional peaks being usually integer multiples of the base frequency. Spectral harmonic peaks are often observed in LFP and EEG/MEG recordings. For instance, a spectral peak in  $\beta$ -frequency range has been found to be exactly twice the individual  $\alpha$ -frequency peak [17–19].

The waveform of oscillations is also important for the understanding of non-linear neuronal interactions, which can be carried out not only within the same frequency band (e.g.,  $\alpha$ ,  $\beta$ ,  $\gamma$ ) but also across different bands. In this case they are referred to as cross-frequency interactions and describe a mechanism through which spatially and spectrally distributed information can be integrated in the brain [20]. The extent to which the presence of such cross-frequency interactions can be due to spurious effects, particularly due to non-sinusoidal waveform of oscillations is being debated [21–23].

Furthermore, a description of oscillations which takes into account their non-sinusoidal waveform has implications for the understanding of oscillatory phase. Oscillatory phase is important in theories of neuronal processing [24–26], reflecting a change in membrane potential for many synchronous neurons. This in turn results in changes in cortical excitability, which has been associated with periodic inhibition. A non-sinusoidal waveform is associated with a deviation from a 50% duty cycle and with a non-uniform phase velocity [27]. This in turn would lead to non-uniform changes in cortical excitability and subthreshold stimulus detection rates along the oscillation cycle.

Here, we investigate measures for quantifying non-sinusoidality in the time domain, with simulation and analysis primarily focused on  $\alpha$ - and  $\beta$ -oscillations in EEG recordings. The aim of the present study is to show that the degree of non-sinusoidality in oscillations may depend on the spatial mixing of the neuronal sources reflected in EEG/MEG/LFP recordings. Depending on synchronization strength and the temporal delay between neuronal populations, the resulting waveform of oscillations can vary from strongly non-sinusoidal to sinusoidal. Spatial mixing will influence measures such as amplitude envelope correlations and  $\alpha/\beta$ -ratio, as different temporal delays will cancel or enhance different frequency components of the non-sinusoidal waveform. Moreover, this might lead to spurious inferences about cross-frequency interactions, which may rather relate to changes in the waveform reflecting in turn changes in spatial synchronization.

## Materials and methods

### Participants

The study protocol conformed to the Declaration of Helsinki and by the ethics committee at the medical faculty of the University of Leipzig (reference number 154/13-ff). The EEG data were previously collected as part of the “Leipzig Cohort for Mind-Body-Emotion Interactions” data set (LEMON) [28]. Written informed consent was obtained prior to the experiment from all participants. Data from 13 participants were excluded due to missing event information, different sampling rate, mismatching header files or insufficient data quality. Additionally, data from 17 participants was excluded for insufficient signal-to-noise ratio (see section Data analysis and Statistics). This resulted in data sets from 186 participants (117 male, 69 female, age range: 20–70 years) with no history of neurological disease and usage of CNS drugs.

### EEG setup

Scalp EEG was recorded from a 62-channel active electrode cap (ActiCAP, Brain Products GmbH, Germany), with 61 channels in the international 10-20 system arrangement and one additional electrode below the right eye recording vertical eye movements. The reference electrode was located at electrode position FCz, the ground was located at the sternum. Electrode impedance was kept below 5 k $\Omega$ . Data were acquired with a BrainAmp MR plus amplifier (Brain Products GmbH, Germany) at an amplitude resolution of 0.1  $\mu$ V with a bandpass filter between 0.015 Hz and 1 kHz and with a sample rate of 2500 Hz. The recordings were performed in a sound attenuated EEG booth.

The experimental session was divided into 16 blocks, each lasting 60 s, with two conditions interleaved, eyes closed (EC) and eyes open (EO), starting in the EC condition. Participants were instructed to fixate on a digital fixation cross during EO blocks. Changes between blocks were announced with the software Presentation (v16.5, Neurobehavioral Systems Inc., USA). Only data from the EC condition were used for analysis.

## Data analysis and computational modelling

**Measures for assessing non-sinusoidality.** To exploit the vast richness of the momentary EEG-signal, we utilize measures of waveform shape in the raw signal with only limited band-pass filtering. The waveform features of an asymmetric signal are illustrated in Fig 1. The crest period  $T_c$  is defined as the time from up-crossing to the next down-crossing. Conversely, the trough period  $T_t$  is the time from down-crossing to next-up-crossing. Each period is associated with two amplitude values, the crest amplitude  $A_c$  and the trough amplitude  $A_t$ . We propose to assess the non-sinusoidality of a signal by considering the ratio of the crest period versus the trough period  $\frac{T_c - T_t}{T_c + T_t}$ , termed CT-difference. The more this value deviates from 0, the more non-sinusoidal the signal is. For more stable estimation, this can be done over several segments of data, with  $\Delta CT = \frac{\text{mean}(T_c - T_t)}{\text{mean}(T_c + T_t)}$ . To compute  $T_c$  and  $T_t$ -values for empirical as well as synthetic data, we used the WAFO toolbox [11], originally developed for the analysis of ocean waves. For computation of  $\Delta CT$ , EEG data were bandpass filtered in the frequency band 3–45 Hz (Butterworth, filter order = 4). As  $\alpha$ - and  $\beta$ -oscillations are used as primary examples in this article, the band-width of the filter was chosen accordingly to minimize zero-crossing distortions by low-frequency drifts. We used all periods with associated pooled crest and trough amplitudes larger than the 50<sup>th</sup> amplitude percentile in order to avoid a contamination with 1/f-noise in EEG signals. Similar measures for the description of oscillatory waveform have also been proposed by [15].

**Time series simulations.** To study properties of the proposed measures, we employed the following simulation procedure: First, basis functions with an arc-shape waveform were constructed, resembling the non-sinusoidal activity of a source. The waveform is composed of two sinusoids, the  $\alpha$ -component with the base frequency of 10 Hz, and the  $\beta$ -component with a frequency of 20 Hz [29]. The sinusoids have a fixed phase shift relative to each other, the power of the  $\beta$ -component is four times smaller than the  $\alpha$ -component:  $\mu(t) = A_1 \cdot \sin(f \cdot 2\pi \cdot t) + A_2 \cdot \sin(2f \cdot 2\pi \cdot t + \psi)$ , with  $A_1 = 1$ ,  $A_2 = 0.25$ ,  $f = 10$  Hz,  $\psi = 1$ . The waveform is asymmetric by construction, see Fig 1 for the waveform and corresponding features. In a second step, signals from  $N$  sources which have a temporal shift  $\phi_i$  relative to each other, with  $\phi_i \sim \mathcal{N}(0, \sigma)$  were added to result in a compound signal  $X(t) = \sum_{i=1}^N \mu(t - \phi_i)$ . The sources represent spatially close neuronal populations participating in the generation of the compound signal. In some cases, the basis signals were amplitude-modulated (resulting in the same amount of amplitude modulation for  $\alpha$  and  $\beta$ -components) to produce amplitude envelopes with a 1/f-distribution as found in real EEG recordings.

## Simulation of $\alpha/\beta$ -ratios and amplitude envelopes

$\alpha/\beta$ -ratios and amplitude envelope correlations were evaluated using the compound signal  $X(t)$ . The compound signal was composed of 20 sources, mixed with temporal delays drawn from a normal distribution with mean 0 and varying values for the standard deviation  $\sigma$ .  $\alpha/\beta$ -ratios were calculated as the ratios of  $\alpha$ - and  $\beta$ -SNR values of the compound signal, evaluated over time series segments of varying length. Here,  $\alpha$ -SNR was taken as oscillatory power at the  $\alpha$ -peak frequency and  $\beta$ -SNR as the oscillatory power at twice that frequency. Power was computed by FFT, Hann window, 1 s window length, 50% overlap. To investigate time courses between  $\alpha$ - and  $\beta$ -components of the compound signal, we calculate correlations between their amplitude envelopes. Amplitude envelopes were calculated by individually bandpass-filtering the compound signal in the base frequency range and first harmonic frequency range  $\pm 2$  Hz, respectively (Butterworth, filter order = 9). Amplitudes envelopes were determined for each frequency band by the means of the Hilbert transform. Then, the Spearman rank

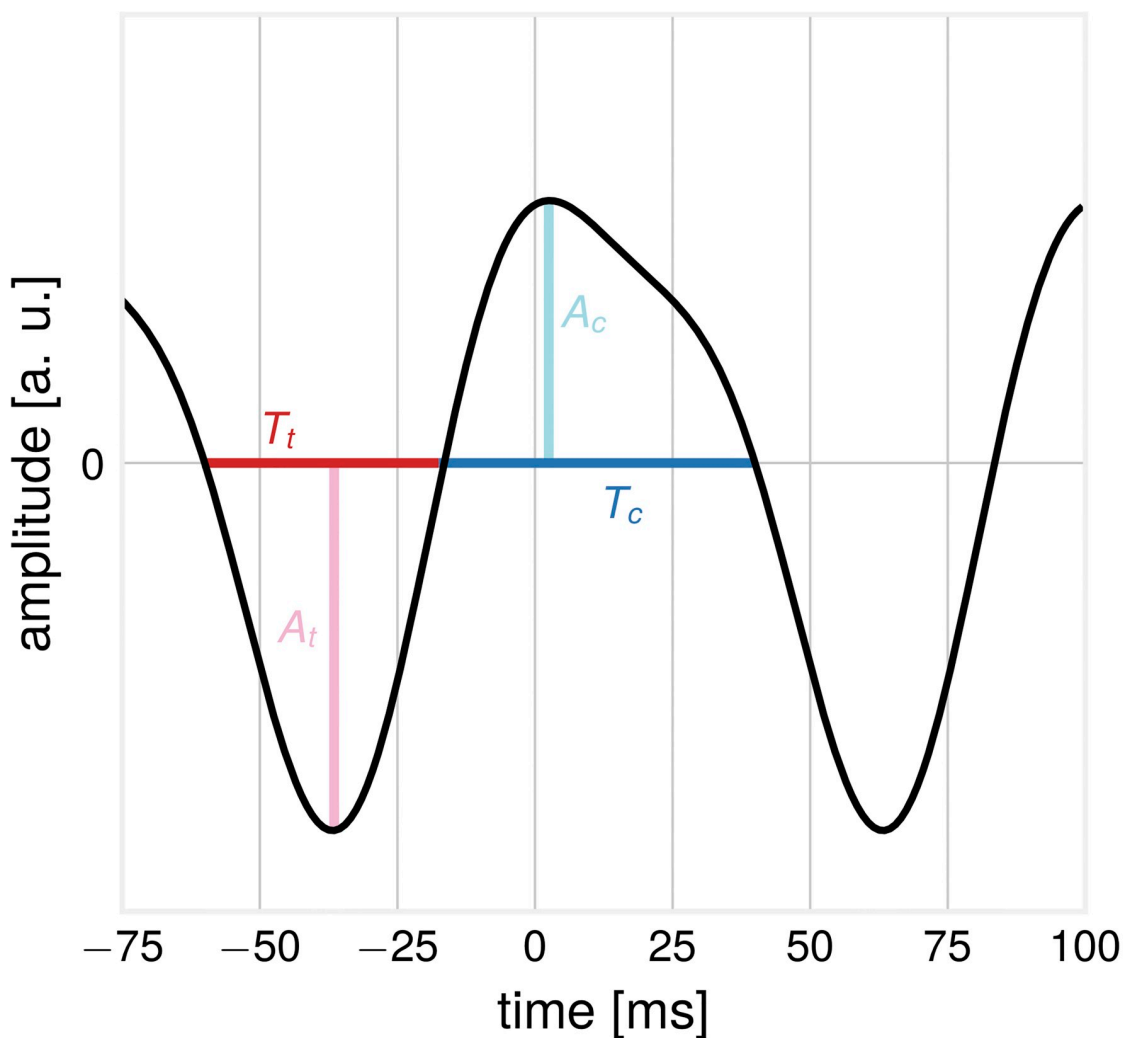


**Fig 1. Illustration: Features of a non-sinusoidal waveform.** The trough period  $T_t$  and the associated trough amplitude  $A_t$  and the crest period  $T_c$  and associated crest amplitude  $A_c$ .

<https://doi.org/10.1371/journal.pcbi.1007055.g001>

correlation coefficient was calculated between  $\alpha$ - and  $\beta$ - amplitude envelopes. The calculation was repeated 1000 times, every time using a new instantiation of the compound signal, sampling new temporal shifts and  $1/f$ -noise for amplitude modulation.

**EEG data analysis and statistics.** The BBCI toolbox [30] was used for EEG data analysis. The data were downsampled from 2500 Hz to 250 Hz, bandpass filtered in the frequency range 1–45 Hz (Butterworth filter, filter order 4). Visual inspection was utilized to exclude outlier channels with frequency shifts in voltage and poor signal quality and data intervals with extreme peak-to-peak deflections or large bursts of high frequency activity. Principal component analysis (PCA) was used for dimensionality reduction by keeping PCs that explain 95% of the total data variance. Next, independent component analysis (ICA) based on the Extended Infomax [31] algorithm was performed (step size:  $0.00065/\log(\text{number of channels})$ , annealing policy: when weight change  $> 0.000001$ , learning rate is multiplied by 0.98, stopping criterion maximum number of iterations 512 or weight change  $< 0.000001$ ). Components reflecting eye movement, eye blink or heartbeat related artifacts were removed. Remaining independent

components (mean number: 21.4, range: 14–28) were projected back to sensor space for further analysis.

As we are interested in oscillatory activity, only participants with sufficient signal-to-noise ratio in the  $\alpha$ -band were included. To determine this, EEG time series were spatially filtered with a Laplacian filter, and the frequency spectrum (FFT, Hann window, 1 s window length, 50% overlap) was computed. The SNR-values of spectral peaks in the  $\alpha$ -band (8–13 Hz) were considered with the  $1/f$ -component removed by fitting a polynomial function to the computed spectrum and subtracting the estimated  $1/f$ -fit [29]. Participants were included if at least one channel displayed a SNR > 5 dB in the  $\alpha$ -band, as evaluated over the whole recording length. Examples of  $1/f$ -corrected spectra can be seen in supplementary material, S1 Fig.

The LEMON data set was available with sampling frequency of 250 Hz. To improve estimation of zero-crossing timing, the data was interpolated to a sampling frequency of 1000 Hz (spline interpolation), for 1 millisecond precision of  $T_c$  and  $T_r$ -values. For the extraction of oscillatory components, spatial-spectral decomposition (SSD) [32] was used. SSD is a method for extraction of cortical sources using Eigenvalue decomposition of channel covariance matrices. It maximizes the oscillatory power of the component at a target frequency band, while minimizing at neighbouring frequency bands. This effectively leads to the extraction of oscillatory components with the strongest SNR. SSD can be computed fast and reliably extracts oscillatory components even for low SNR. The frequency band of interest was identified as the subject-individual spectral peak in  $\alpha$ -frequency range  $\pm 2$  Hz. Although SSD is trained on a narrowband process, we then applied obtained SSD spatial filters on broadband data. The main idea here is that if the fundamental frequency and its harmonics belong to the same spatial source, then the projected component should have a frequency spectrum displaying corresponding  $\alpha$ - and  $\beta$ -peaks. If  $\beta$ -oscillations indeed originate from the same source as  $\alpha$ -oscillations (this would be the case for non-sinusoidal signals) the application of SSD spatial filtering would result in the extraction of not only  $\alpha$ - but also  $\beta$ -oscillations. Using the same spatial filter for all frequencies ensures that the extraction of different spectral components is not individually optimized thus reducing the extraction of spatially different neuronal sources. For comparison, the analysis was also performed with fastICA (non-linearity:  $u^3$ , epsilon: 0.0001, number of maximum iterations: 1000).

For demonstrations, we generated synthetic compound signals from data by adding extracted SSD components with a varying time shift. Empirical  $\alpha/\beta$ -ratios were calculated as the ratio of  $\alpha$ - and  $\beta$ -SNR values, evaluated over segments of varying time length. The subtraction of  $1/f$ -fit was not performed here, as its estimation becomes unstable for segments of short length. Amplitude envelopes were calculated with the same parameters as for the synthetic compound signals.

## Results

### Waveforms become more sinusoidal with increased temporal delays between sources

Spatial mixing of non-sinusoidal sources results in more sinusoidal compound signals. Considering the example in Fig 2A, seven basis signals are added with temporal delays drawn from a normal distribution. The compound mean signal has lost its asymmetrical shape and shows no difference between crest and trough periods (shown for one oscillation cycle in Fig 2B), compared to the basis functions. Note that the disappearance of the non-sinusoidal waveform is not due to the changes in SNR but due to the time delay between individual sources. As a temporal delay of e.g. 10 ms is equivalent to  $\frac{1}{5}\pi$  for the  $\alpha$ -component, but twice as large,  $\frac{2}{5}\pi$  for the  $\beta$ -component, this leads to faster attenuation of the  $\beta$ -component.

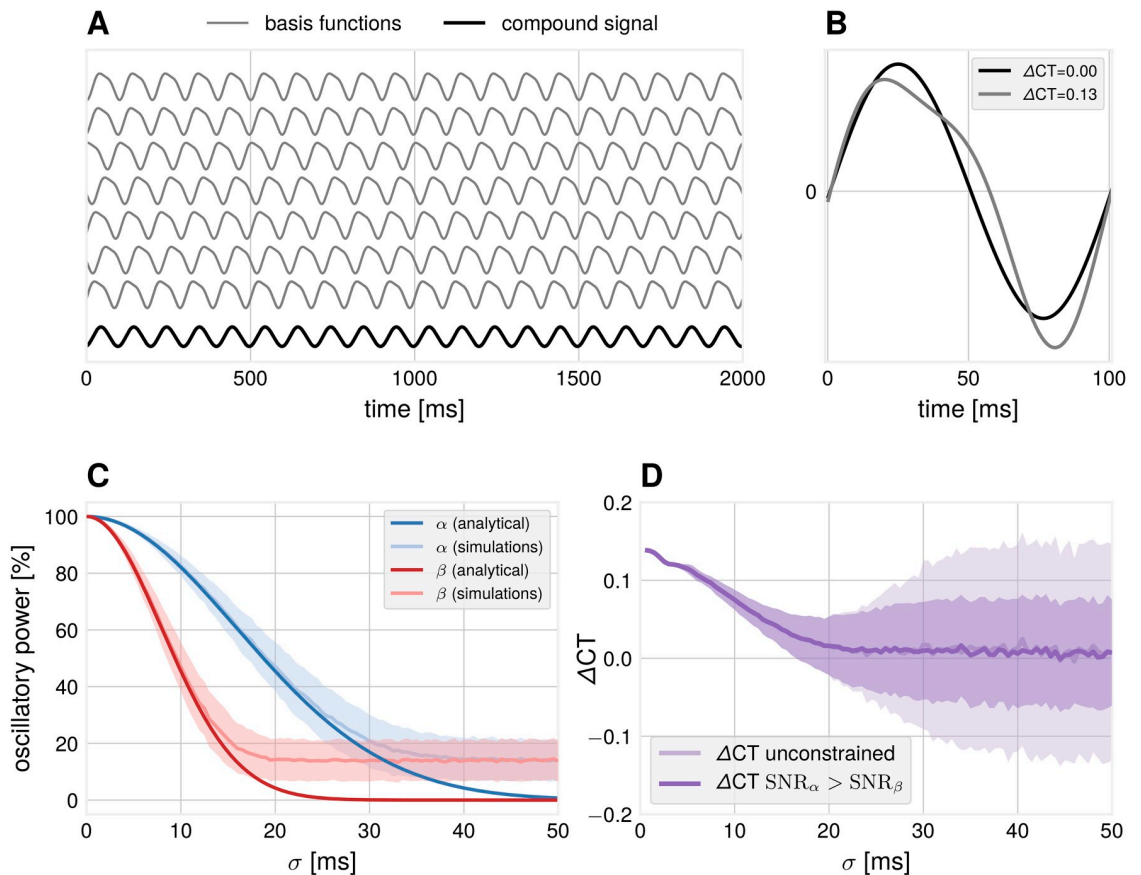


**Fig 2. Simulation: Dependence of waveform measures on spatial mixing.** (A) Illustration how non-sinusoidal waveforms add up to a more sinusoidal compound signal if they are shifted with respect to each other with a certain standard deviation  $\sigma$  (example for  $\sigma = 30$  ms). (B) Examples of one cycle of source and compound waveforms and their respective zero-crossings with associated  $\Delta CT$  values. (C) The relative power of the two frequency components of the compound signal as evaluated from the Fourier spectrum. The  $\beta$ -component attenuates faster than the  $\alpha$ -component. Number of iterations = 1000. Number of sources = 40. Error bars indicate  $\pm 1$  SD. In simulations, the obtained power for large temporal delays is constrained by the finite number of generators used and results in a deviation from the analytical solution. (D)  $\Delta CT$  for the compound signal drops as a function of the standard deviation  $\sigma$ . In unconstrained simulations,  $SNR_{\beta}$  can get larger than  $SNR_{\alpha}$ , resulting in high values of  $\Delta CT$ . Number of iterations = 1000. Error bars indicate  $\pm 1$  SD.

<https://doi.org/10.1371/journal.pcbi.1007055.g002>

To quantify the attenuation of the faster component, we computed the power spectrum of the compound signal  $X(t)$  by the Fourier transform as a function of standard deviation of the temporal delays  $\sigma$ . The analytical solution is proportional to  $\exp(-2(\pi \cdot \sigma \cdot f)^2)$ , as obtained by Fourier analysis of the compound signal as a function of  $\sigma$ . The quadratic dependency on the frequency term results in a faster attenuation of higher frequencies, as seen in Fig 2C. This results in a more sinusoidal signal for larger values of  $\sigma$ . Not only spectral power, but also the proposed measure for non-sinusoidality in the temporal domain is able to detect non-sinusoidality in the compound signal as a deviation from 0 (see Fig 2D). In our unconstrained simulations, the spectral peak of the  $\beta$ -component can be higher than the spectral peak of the  $\alpha$ -component (see also later sections in the Results). In this case, extreme  $\Delta CT$  values are observed, leading to an increased standard deviation for large temporal delays. The implication is that the degree of non-sinusoidality present in the waveform can serve as an indicator of spatial synchronization. It can also constrain the mixing coefficients, which are known in simulations, but are not known for real EEG recordings.

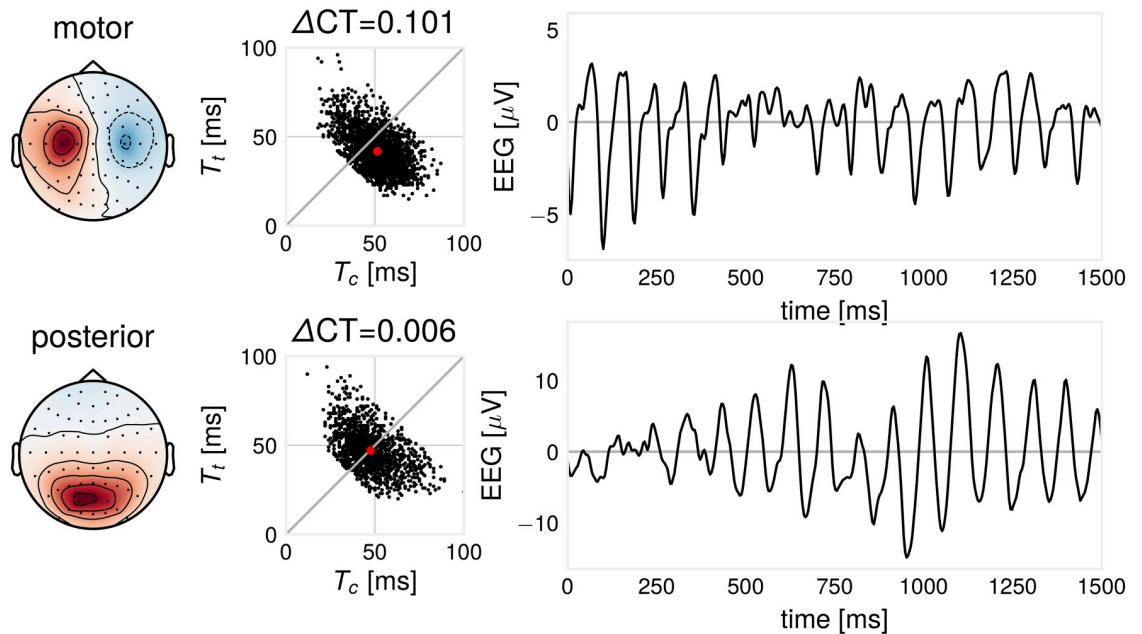


**Fig 3. Illustration:  $\Delta CT$  differs for two EEG oscillatory components.** Components extracted for one participant. Left: SSD component pattern. Middle: for every oscillatory cycle, there are two corresponding  $\Delta CT$  and  $T_c$ - and  $T_t$ -values. Red dot indicates mean  $T_c$ - and  $T_t$ -values. Right: example time course excerpt of the signal. In this case, the motor component shows a characteristic arc-like shape with larger non-sinusoidality than the posterior component.

<https://doi.org/10.1371/journal.pcbi.1007055.g003>

As an example for the  $\Delta CT$ -measure, we illustrate the  $T_c$  and  $T_t$ -distributions for different types of EEG oscillations in the 8–13 Hz frequency band for an exemplary participant. After SSD decomposition, one motor and one visual component was identified from the associated activation patterns. We compute  $T_c$  and  $T_t$  for motor and posterior oscillations, shown in Fig 3. In this participant, a more non-sinusoidal oscillation can be found for the motor-component. The motor component is typically described as arc- or comb-shaped [33, 34] and the posterior  $\alpha$ -component as symmetric [35]. Using a measure such as  $\Delta CT$  can quantify waveform shape and shows that also posterior  $\alpha$ -oscillations can also be of non-sinusoidal shape in line with [29]. We provide more evidence to demonstrate the non-sinusoidal nature of  $\alpha$ -oscillations, see supplementary material, S2 Fig.

### Demixed recordings show higher degree of non-sinusoidality

We quantified the extent to which  $\Delta CT$  is affected by a demixing procedure, which brings sensor signals closer to their sources. For this,  $\Delta CT$  was computed in sensor space recordings for all included participants, as well as for SSD-extracted components. SSD components have a higher  $\Delta CT$  indicating a higher degree of non-sinusoidality across participants ( $p = 5.7 \cdot 10^{-15}$ , two-sided Wilcoxon signed rank test), as illustrated in Fig 4. We additionally ran our analyses using fastICA instead of SSD. The results are comparable to SSD, with fastICA achieving a higher  $\Delta CT$  compared to sensor space ( $p = 8.86 \cdot 10^{-4}$ , two-sided Wilcoxon signed rank test).

The dependence of the  $\Delta CT$  of SSD-components to SNR was assessed by computing the SNR in the  $\alpha$ -frequency band via  $1/f$ -corrected spectrum and absolute value of  $\Delta CT$  for all SSD-components with  $\alpha$ -SNR > 5 dB. We found a correlation of .242 (Spearman's rho,  $p < 6.99 \cdot 10^{-31}$ ) of absolute  $\Delta CT$  with  $\alpha$ -SNR, with more non-sinusoidal signals as measured by  $\Delta CT$  for higher SNR. Resorting the absolute  $\Delta CT$ -values according to their associated

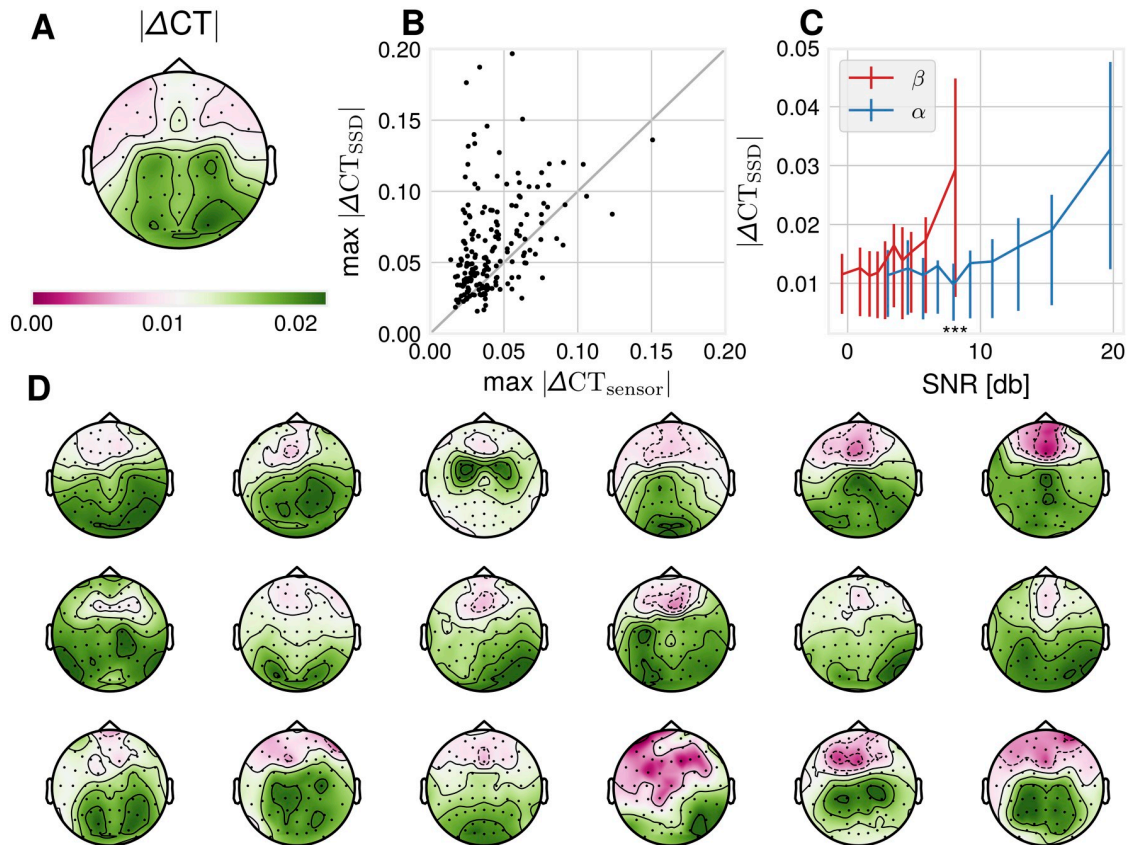


**Fig 4. Data analysis: Empirical  $\Delta CT$ -distributions.** (A) absolute  $\Delta CT$  across participants computed from sensor space data, plotted topographically. (B) Maximal SSD absolute  $\Delta CT$  is larger than sensor space absolute  $\Delta CT$  across participants,  $N = 186$ ,  $p = 5.7 \cdot 10^{-15}$ , two-sided Wilcoxon signed rank test. (C) Binned  $\alpha$ -SNR and  $\beta$ -SNR as estimated from  $1/f$ -adjusted spectrum versus mean absolute  $\Delta CT$  in that bin. Error bars are 25<sup>th</sup> – 75<sup>th</sup> percentile value ranges for absolute  $\Delta CT$  for the respective bin. Wilcoxon signed rank test between absolute  $\Delta CT$ -values corresponding to the 10<sup>th</sup> bin of  $\beta$ -SNR and 5<sup>th</sup> bin of  $\alpha$ -SNR: p-values:  $5.40 \cdot 10^{-18}$ . (D) 18 single subject absolute  $\Delta CT$ -topoplots examples show substantial variability of spatial  $\Delta CT$ -distribution. Participants were selected according to the number of channels satisfying the SNR-criterion of 5 dB, so a topography is visible.

<https://doi.org/10.1371/journal.pcbi.1007055.g004>

$\beta$ -SNR values shows that a  $\beta$ -SNR-level of the same magnitude as  $\alpha$ -SNR of e.g.  $\sim 8$  dB is associated with higher  $\Delta CT$  values. In other terms, a pronounced  $\beta$ -peak in the  $1/f$ -corrected spectrum corresponds to a higher degree of non-sinusoidality than an  $\alpha$ -peak of the same magnitude. This observation is in agreement with our simulations presented above indicating that the presence of  $\beta$ -oscillations defines non-sinusoidality of the waveform.

The topographic distribution of  $\Delta CT$ -values can be seen in Fig 4D, which shows considerable variation across participants. Although the group average in Fig 4A shows increased values for both central-motor and occipital channels, on a single subject level either a central-motor or an occipital maximum is rather visible. In sum, the non-sinusoidality of EEG recordings is affected by spatial mixing of oscillatory sources and also by SNR in relation to  $1/f$ -noise.

### Constructive and destructive interference with respect to temporal delays

A spatial summation of basis signals with the same spectral content but different temporal delays can have differential consequences for the respective constituent frequencies, enhancing or diminishing respective oscillatory power. We provide three examples for this phenomenon.

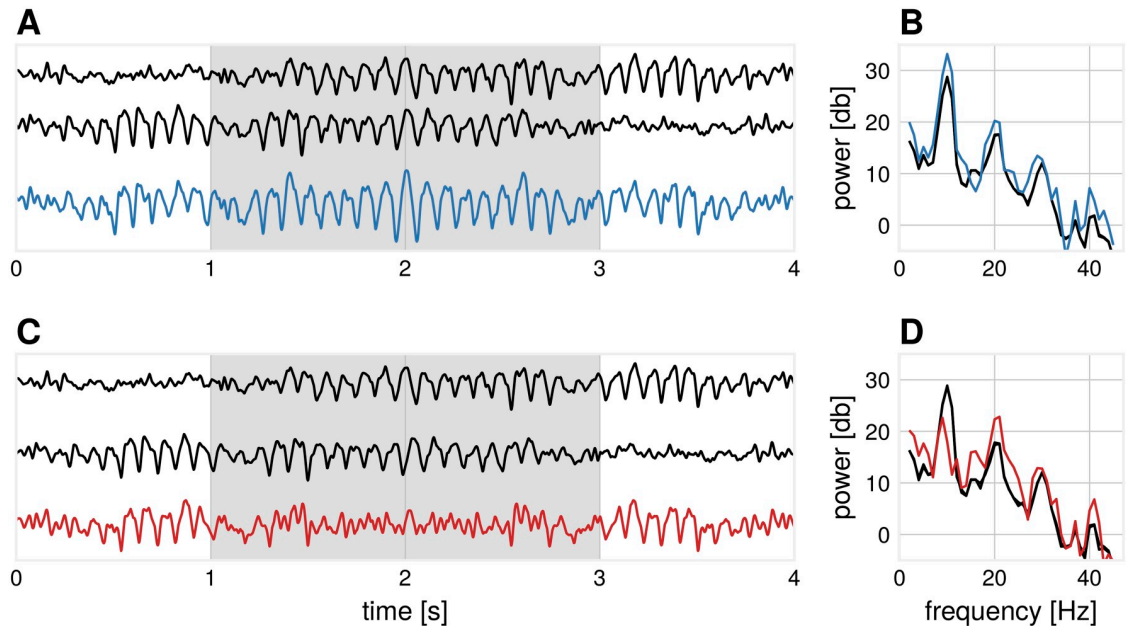


**Fig 5. Illustration: The emergence of  $\beta$ -events from  $\alpha$ -dominated sources.** (A) Two basis functions (black) mix with a temporal delay ( $\sigma = 15$  ms) such that the  $\alpha$ -power is enhanced in the compound signal (blue) during the segment marked in gray. (B) The corresponding power spectrum of the segment marked in gray for subplot (A) for basis functions (black) and compound signal, where both  $\alpha$ - and  $\beta$ -spectral peaks are enhanced (blue). (C) Two basis functions (black) mix with a temporal delay ( $\sigma = 43$  ms) such that the  $\alpha$ -power is diminished in the compound signal (red) during the segment marked in gray. (D) The corresponding power spectrum of the segment marked in gray for subplot (C) for basis functions (black) and compound signal, where the  $\alpha$ -peak is largely diminished and  $\beta$ -peak is enhanced (red).

<https://doi.org/10.1371/journal.pcbi.1007055.g005>

**Attenuation of the  $\alpha$ -component and enhancement of the  $\beta$ -component.** Non-sinusoidal signals can mix in such a way that the more prominent  $\alpha$ -component is attenuated, while higher harmonics are preserved. This will lead to the emergence of  $\beta$ -events in the compound signal without the strong presence of  $\alpha$ -events, even though the original source signals still have a high amount of  $\alpha$ -frequency spectral content. Fig 5 shows two basis segments of real EEG recordings which have the same spectral content (the bottom one is the time-reversed version of the top one), which are added with varying temporal delays. Depending on this delay, this results in periods in the compound signal where the  $\alpha$ -component is diminished, and a higher amount of  $\beta$ -spectral content emerges. This phenomenon is most pronounced if the temporal delay is approaching  $\pi$  of the base oscillation (i.e. destructive interference), which corresponds to  $2\pi$  for the first harmonic (i.e. constructive interference). The origin of the  $\beta$ -rhythm is debated [36], with recent investigations showing that  $\beta$ -oscillations occur in bursts [37], not in continuous form. Until now,  $\beta$ -oscillations is only treated as a harmonic of  $\alpha$ -oscillations, when  $\alpha$ -oscillations are present. We show that there could be instances over short time periods, where strong  $\beta$ -oscillations can arise through spatial summation, without a visible  $\alpha$ -component in the compound signal. As a general rule of thumb, we recommend that  $\beta$ -oscillations should be analyzed in conjunction with  $\alpha$ -oscillations, especially when the peak  $\beta$ -frequency is exactly twice the peak  $\alpha$ -frequency, indicating a harmonic relationship, whereas a non-integer relationship of  $\alpha$ - and  $\beta$ -frequency is indicative of independent sources.

**Influence of temporal delays on  $\alpha/\beta$ -ratios.** Next, we show the impact of spatial synchronization on  $\alpha/\beta$ -ratios in a simulation with a higher number of source basis signals, each having identical spectral content. As the temporal delay between source signals increases, a spread in  $\alpha$ - and  $\beta$ -SNR becomes visible, as shown in Fig 6. This is the same phenomenon as visible in

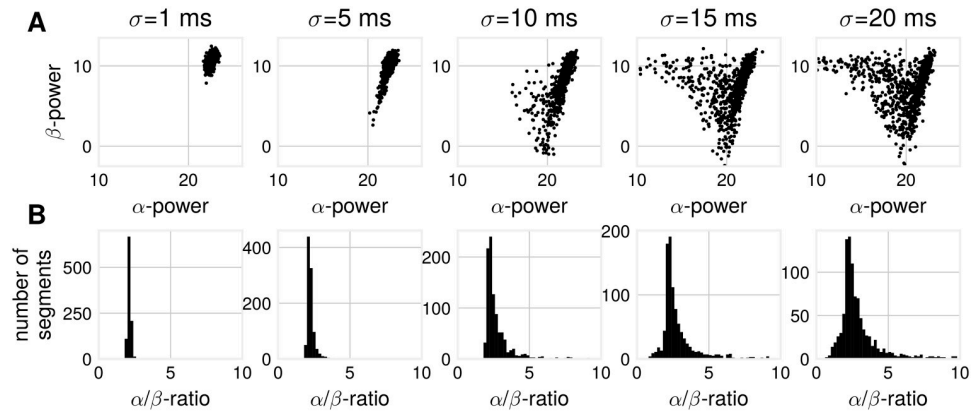


**Fig 6. Simulation:  $\alpha/\beta$ -ratios change with increased mixing time lags.** (A)  $\alpha$ - vs.  $\beta$ -power for compound signals composed of non-sinusoidal basis signals for varying standard deviations of the time shift. Spread in power is larger for larger time shifts. Each point signifies  $\alpha$ - and  $\beta$ -power as computed from one compound signal. (B) This results also in a spread of  $\alpha/\beta$ -ratios as constructed from  $\alpha$ - and  $\beta$ -power. Number of generators: 20, number of iterations: 1000, segment length = 5 s.

<https://doi.org/10.1371/journal.pcbi.1007055.g006>

Fig 2C, where one sees a diminishing difference in oscillatory power for  $\alpha$ - and  $\beta$ -components with increased temporal mixing delay. The subplots in Fig 6 can be considered as detailed representations of the amplitude-ratio distribution corresponding to points taken from x-axis in Fig 2. From these subplots one can see that with the increase of the temporal delays between non-sinusoidal sources the power of  $\beta$  in proportion to  $\alpha$  grows which in turn can lead to instances where primarily  $\beta$ -oscillations will be visible.

A mixture of a larger number of source signals can yield a change in spectral content of the compound signal, even without any changes in the spectral content of the source basis signals. This has implications for measures relating oscillatory power of two frequencies, for instance  $\alpha/\beta$ -ratio. Changes in these measures may not necessarily reflect changes in spectral content, but a change in temporal coupling of non-sinusoidal signals.

$\alpha/\beta$ -ratios were also computed for real EEG recordings. A spread in these ratios is visible, see Fig 7A. Considering segments of short length, periods where  $\beta$ -power is larger than  $\alpha$ -power results in  $\alpha/\beta$ -ratios  $< 1$ . To summarize, in agreement with the simulations, we show that obtaining larger  $\beta$ -power than  $\alpha$ -power is also possible in real EEG data and this phenomenon can be observed more often when considering shorter segments (Fig 7B).

#### Influence of temporal delays on amplitude envelope cross-frequency correlations.

Another result of differential attenuation of separate frequency bands is that correlations between amplitude envelopes across frequencies are influenced by spatial synchronization. An argument for the separation of  $\alpha$ - and  $\beta$ -rhythms into individual components (not stemming from non-sinusoidal waveform) is that only weak amplitude envelope correlations [38] can be found. The argument states that if they originate from the same cortical source, amplitude envelope correlations must be strong. We show that amplitude envelope correlations can vanish due to the non-trivial phase cancellation effects in non-sinusoidal signals. The signal is attenuated to a different degree for the constituting frequency components of the non-sinusoidal base signals. As a result, such attenuation can lead to no correlation between the corresponding envelopes or even to a negative correlation. In line with previous studies about the spurious effects of non-sinusoidal oscillations [21–23] these effects of spatial summation provide further cautionary. In simulations, we analyzed amplitude envelope correlations between  $\alpha$ - and  $\beta$ -components, extracted with the corresponding band-pass filtering. Even though the basis functions were generated as a non-sinusoidal waveform with fixed phase delay between

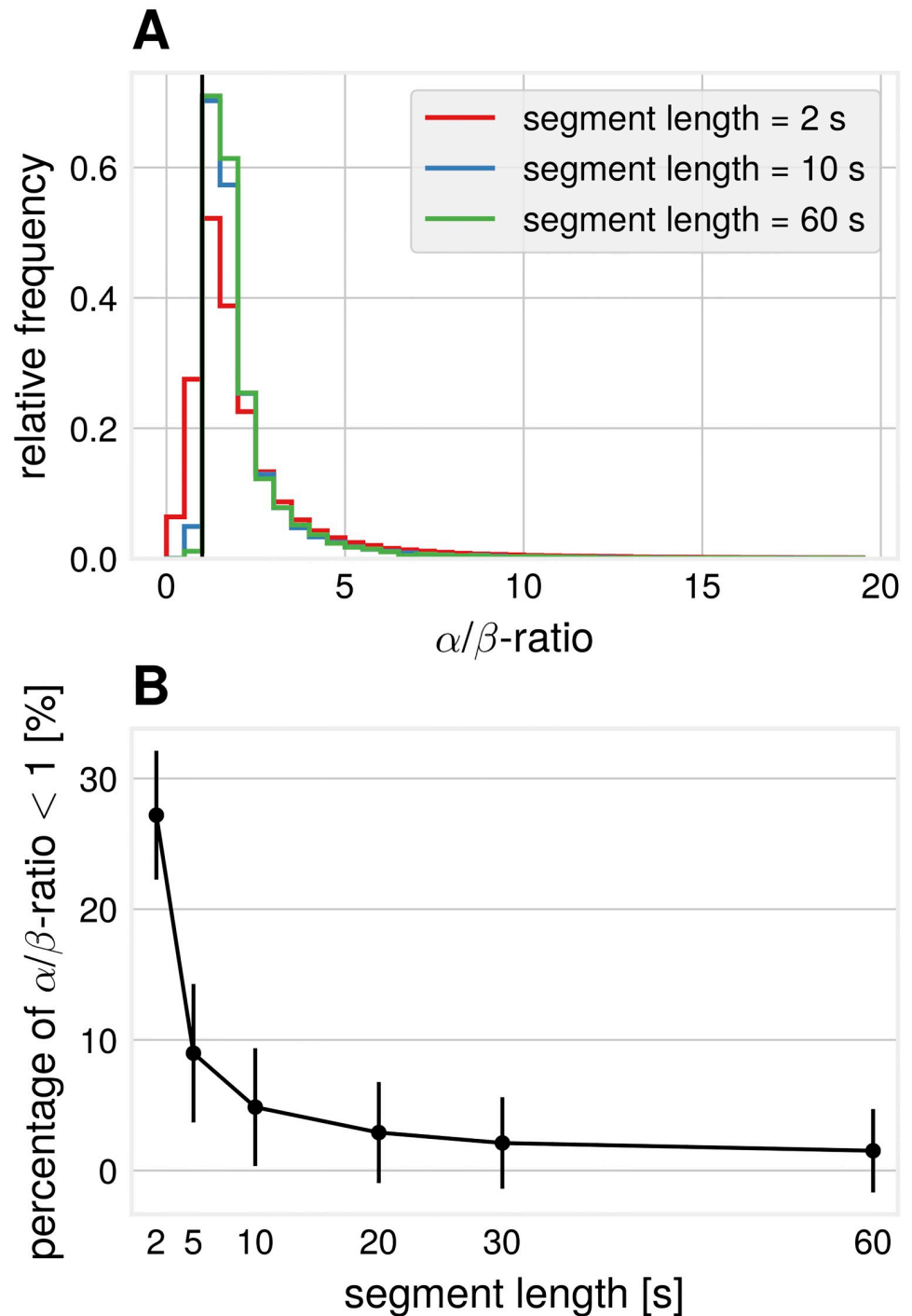


**Fig 7. Data analysis: Empirical  $\alpha/\beta$ -ratios.** All SSD components from all participants pooled. (A)  $\alpha/\beta$ -ratios for different segment lengths, pooled over segments. (B) Percentage of  $\alpha/\beta$ -ratio < 1 (i.e.  $\beta$ -SNR is higher than  $\alpha$ -SNR) for different segment lengths.

<https://doi.org/10.1371/journal.pcbi.1007055.g007>

the two rhythms, a range of very different correlation values can be observed for individual segments of the compound signal (i.e. a simulation of synthetic EEG data). Fig 8A shows exemplary time courses for large positive and surprisingly even negative  $\alpha$ - vs.  $\beta$ -correlations. These negative correlations can not be predicted from the amplitude dynamics of individual

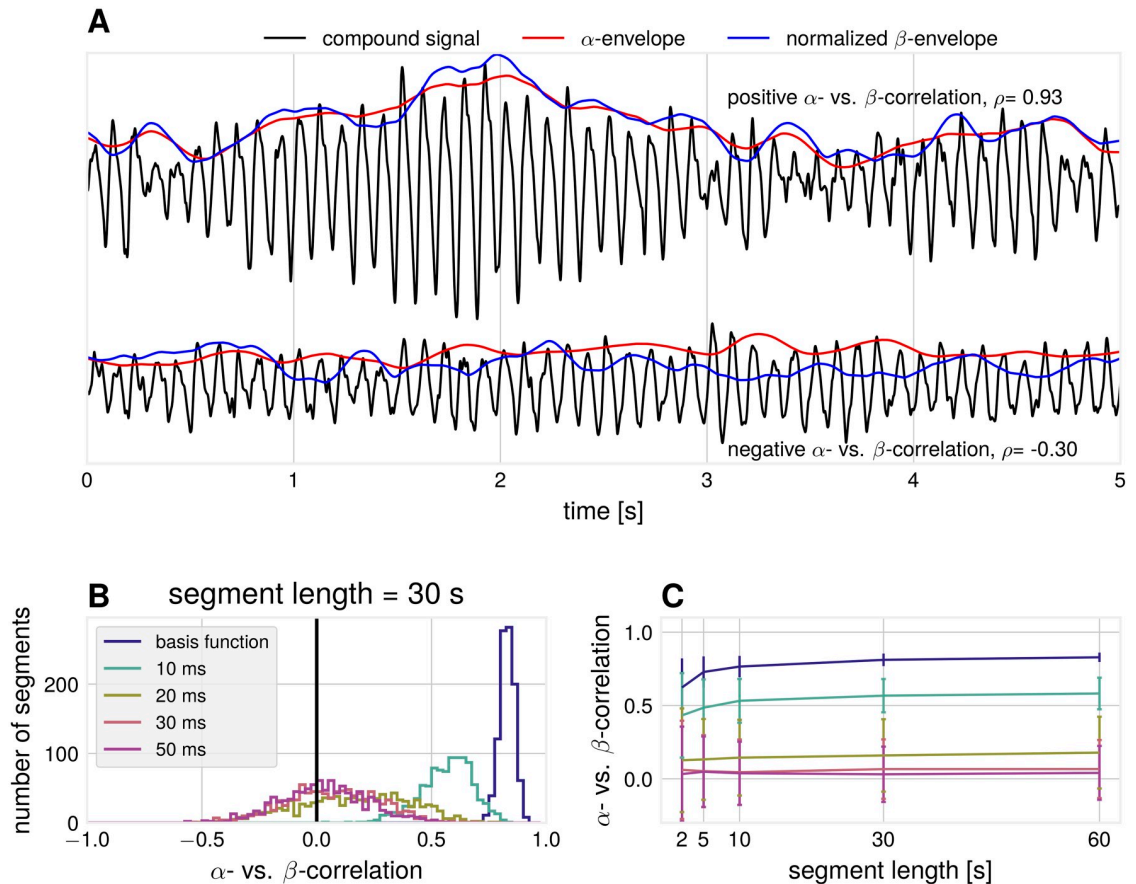


**Fig 8. Simulation: Relationship between  $\alpha$ - and  $\beta$ -envelopes.** (A) Examples for compound signals with positive (top) and negative (bottom)  $\alpha$ - vs.  $\beta$ -envelope correlations. The  $\beta$ -envelope was scaled to aid comparisons to the  $\alpha$ -envelope ( $\sigma = 10$  ms, segment length = 5 s) (B) Spearman rank correlation between synthetic  $\alpha$ - vs.  $\beta$ -envelope time courses over 1000 independent segments. Number of generators = 20. (C) The average correlation as a function of the segment length and standard deviation of the time shift between basis functions.

<https://doi.org/10.1371/journal.pcbi.1007055.g008>

sources as they only have positive correlations by construction. The observed correlations are dependent on the standard deviation of the mixing coefficient distribution, as illustrated in Fig 8B, with negative correlations emerging with the increase of the standard deviation of mixing coefficients. The shown examples are for a fixed segment length, but Fig 8C shows that the effect is present for different lengths of segments.

To validate predictions from simulations, we also quantified  $\alpha$  vs.  $\beta$  amplitude envelope correlations in empirical data. Fig 9 shows that amplitude envelope segments as extracted by SSD display larger positive correlations compared to sensor space amplitude envelope correlations. The figure also shows the presence of negative correlations in agreement with the predictions from simulations. Note that with smaller segments one can observe more and stronger negative correlations due to their transient nature.

## Discussion

In this study we investigated how spatial neuronal synchronization can influence the waveform of neuronal oscillations, affect  $\alpha/\beta$ -ratios and  $\alpha$ - vs.  $\beta$ -envelope relations. Compound signals become more sinusoidal than their sources for a certain range of temporal delays. We show that the examined measures can be affected solely by these delays even when the basic

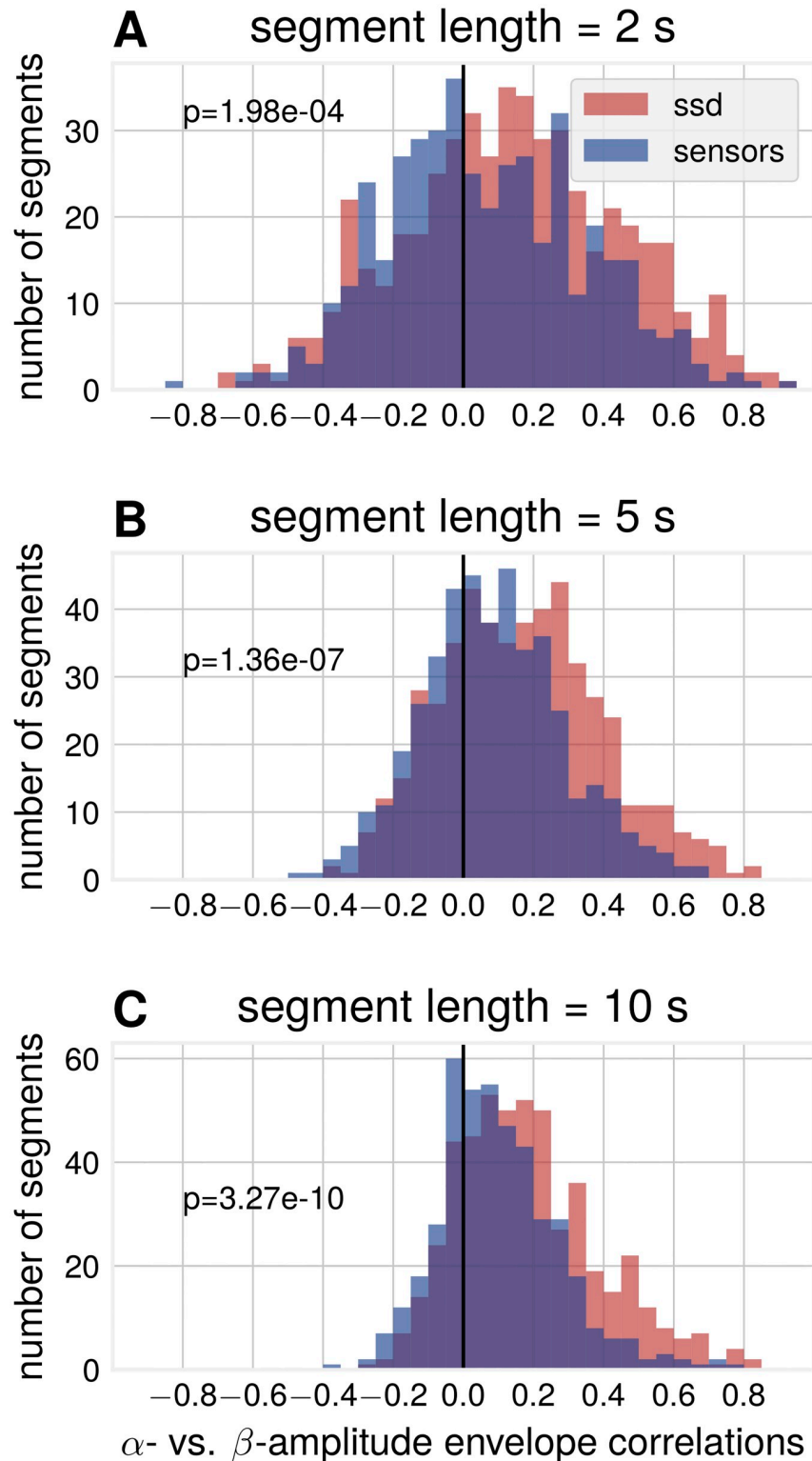


**Fig 9. Data analysis: SSD components show increased correlations between  $\alpha$ - and  $\beta$ -envelope time courses compared to sensor space.** Subplots are for different segment lengths, (A) 2 s (B) 5 s (C) 10 s. Three sensor space channels (C3, C4, Oz) and three SSD components for each participant, pooled over participants, p-values for Wilcoxon rank sum test ( $N_{SSD} = 464$ ,  $N_{sensors} = 374$ ).

<https://doi.org/10.1371/journal.pcbi.1007055.g009>

waveform and spectrum remain the same for the original sources. Moreover, in short segments,  $\beta$ -SNR can be larger than the  $\alpha$ -SNR, through the attenuation of the base frequency. This in turn might relate to the detection of  $\beta$ -oscillations in EEG/MEG without the concurrent presence of detectable  $\alpha$ -oscillations. This is relevant for the studies using band-ratios as biomarkers, such as  $\theta/\beta$ - or  $\alpha/\beta$ -ratio, as indicators for instance relating to cognitive performance anxiety [39] and attention-deficit/hyperactivity disorder [40]. Also, for event-related desynchronization (ERD), where  $\alpha$ - and  $\beta$ -ERD has been investigated separately, the difference in post-movement rebound time-courses between the two rhythms [41] may not necessarily reflect independent rhythms, but may be a consequence of non-sinusoidal waveform shape. Moreover, many previous studies on  $\beta$ -oscillations reviewed in [1, 36] indicate that these oscillations are involved not only in sensorimotor but also in cognitive functions including working memory and decision making. Given that  $\beta$ -oscillations often participate in these functions by transiently changing their amplitude, the results of our study indicate (especially for short time intervals) that the changes in  $\beta$ -oscillations should always be considered in relation to the dynamics of  $\alpha$ -oscillations.

Regarding the variability in spectral profiles, different scenarios are possible when estimating  $\alpha$ - and  $\beta$ -relationships arising from the non-sinusoidality of waveforms. Importantly, these diverse spectral profiles can arise from the spatial mixture of non-sinusoidal basis signals with the same waveform. As illustrated in Fig 10, for the simple scenario with only two sources, different components of a non-sinusoidal waveform can cancel depending on the temporal delay between them. While we primarily focus in this study on the relationships between  $\alpha$ - and  $\beta$ -oscillations, the results can be generalized to the relationships between oscillations at other frequency bands.

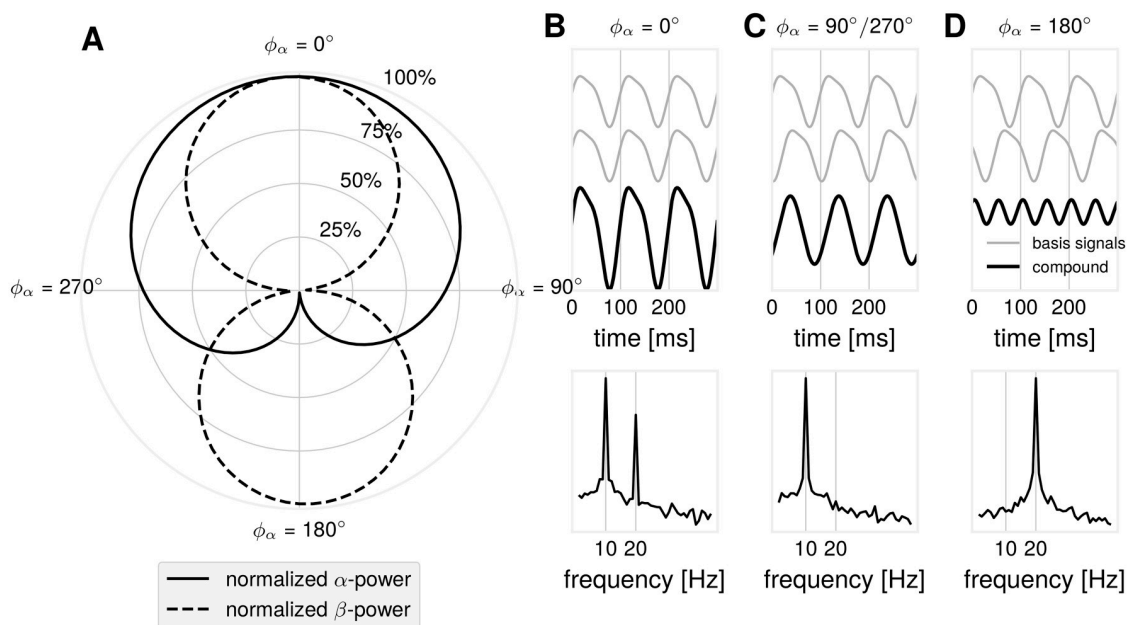


**Fig 10. Illustration: Possible  $\alpha/\beta$ -dynamics as function of the time delay for simple synthetic signals.** Two non-sinusoidal  $\mu$ -wave signals were mixed with varying time delay  $\phi_\alpha$  between them ( $\phi_\alpha = 360^\circ$  is equal to 100 ms, a full cycle of the base  $\alpha$ -frequency oscillation). A full  $\alpha$ -cycle corresponds to two full  $\beta$ -cycles:  $\phi_\alpha = 2 \cdot \phi_\beta$ . (A) A polar plot showing  $\alpha$ - and  $\beta$ -power as a function of the time delay  $\phi_\alpha$ .  $\alpha$ - and  $\beta$ -power decay differentially as a function of the time delay  $\phi_\alpha$ . (B) Time course of the basis signals and the compound signal with the corresponding power spectrum showing maximal  $\alpha$ - and  $\beta$ -power for  $\phi_\alpha = 0^\circ$ . (C) Time course of the basis signals and the compound signal with the corresponding power spectrum showing attenuation of  $\beta$ -power for  $\phi_\alpha = 90^\circ/270^\circ$ . (D) In the case of  $\phi_\alpha = 180^\circ$ , in the compound signal, only the  $\beta$ -component remains when the  $\alpha$ -peaks of first basis signal align the troughs of the second basis signal, causing cancellation.

<https://doi.org/10.1371/journal.pcbi.1007055.g010>

## Limitations

In the present study, we realized the mixing of signals from individual neuronal populations with unitary weights in the simulations. For empirical recordings, data  $B$  recorded with EEG/MEG can in general be represented as  $B = L \cdot J$ , where  $L$  is a lead-field matrix and  $J$  contains dipole currents at different locations. In our simulations, the sources can be assumed to be located close to each other (e.g.  $<5$  mm) and in practical terms their location and orientation could be considered to be approximately the same thus having the same gain in  $L$  matrix. In this way the same gain (unitary or not) for all sources is justified and would lead to similar results. Already on this spatial scale, sources display great dynamical variety [42], with diverse temporal delays [43]. Of course, EEG activity reflects the superposition of a large number of other remote sources, where the mixing of signals at the sensor level would occur with different weights. This, however, would not change one of the main findings of the study qualitatively, namely that the mixing of many non-sinusoidal sources results in more sinusoidal signals.

From our simulations, it follows that if the amplitude weight from one of the sources would be very large (far larger than the weight from other sources), then the signal would remain strongly non-sinusoidal. Only when weights of other multiple sources have sufficient strength and these sources are not synchronized at exactly zero-lag delay [44], only then the superposition of the signals results in more sinusoidal signals. At the level of the remote neuronal populations recorded with EEG, this observation has been confirmed in our study. We showed that  $\Delta CT$  deviated stronger from 0 for SSD components compared to sensor space data since in the latter case effects of the spatial mixing are more pronounced. Consequently, introducing simulations with different spatial weights would only result in superimposed signals having more non-sinusoidal waveform. Even despite relatively simple but neurophysiologically plausible simulations, we are still capable to show the effects of spatial mixing on waveforms and on complex cross-frequency interactions. The model should be sufficiently complex (but not too complex) to capture the phenomenon under study. Nikulin and Brismar (2006) [29] showed that two sinusoids at different frequencies with a specific phase shift and amplitude ratio capture accurately the prototypical shape of non-sinusoidal oscillations recorded in actual EEG experiments. This shape is reproducible across a majority of subjects ( $n = 176$ ) in that study and for central and occipito-parietal regions. Similar simple parametric models with superposition of trigonometric functions have been used to learn the morphology of the  $\mu$ -rhythm for monitoring mental states in brain-computer interfaces [45, 46] or investigating the effects of non-sinusoidal shape on phase-amplitude coupling [47]. A biophysical model could further improve the understanding of how exactly transmembrane currents and kinetic of ion channels lead to the generation of a given wave shape. Typically, neural mass models, where the output macroscale signal is produced through an interplay of excitatory and inhibitory populations, are able to produce signals of non-sinusoidal waveforms [48, 49]. Specifically, for the generation of the sensorimotor  $\mu$ -rhythm, a model on the level of a cortical column with spatially extended neuronal morphologies is able to generate non-sinusoidal source signals through integration of thalamic driving input via basal and apical dendrites of pyramidal neurons [50]. However, once we have an accurate description of the waveform, we can then proceed with the question of what would be the consequences for EEG/MEG/LFP signals when processes with such waveform are mixed with variable time-delays. Although these time delays are not accurately known in advance, we provide a wide range of simulations covering a relatively broad distribution of delays. Therefore, investigating waveform of oscillations can aid in constraining empirical mixing temporal delays.

## Implications

If we assume that the underlying source signals are non-sinusoidal, as evidence from LFP and invasive recordings suggests, the degree of non-sinusoidality present in macroscale EEG and MEG recordings relates to spatial synchronization with small time lags. Non-sinusoidality in EEG/MEG recordings should be present to a higher degree in signals which demonstrate less spatial mixing. This is the case for instance for many LFP recordings where spatial mixing is restricted to local neuronal populations located in the proximity to the recording electrode [13, 14]. Therefore, non-sinusoidality of the oscillations can be used as a proxy for demixing of neuronal signals recorded with EEG/MEG. SSD is based on covariance matrices of narrow band processes. Utilizing a broader spectrum of information content is possible with other methods, for instance by learning a dictionary of canonical waveforms and associated spatial patterns [16] or using bicoherence for localizing non-sinusoidal waveform shape generators [51, 52]. Note that the synchronization index can be 1 for sources having phase lag of 0 or phase lag of  $\frac{\pi}{2}$ . In our study we are not measuring the synchronization strength per se, but rather state that the wide distribution of time delays between sources translates to the degree of non-sinusoidality in the measured neuronal signals. Improved methodology will aid in determining functional properties of oscillations with increased sensitivity (not affected by narrow band-pass filtering) when relating oscillatory component to behavioral and stimulation outputs.

Investigating waveform in the temporal domain may aid in an improved determination of phase. A shortcoming of current methods for the computation of spatial filters which are based on linear decompositions (SSD, CSP, ICA) is that their solutions are invariant with respect to sign/polarity of the extracted signals. It has been shown that brain states associated with specific phases have differential functional consequences for cortical excitability and plasticity [24, 53, 54]. For instance, magnetic stimulation at the trough of the sensorimotor rhythm elicits a higher response compared to stimulation at the peak of the sensorimotor rhythm [53]. In this study, the rhythm of interest was extracted with a local spatial filter using a fixed electrode set, which is agnostic to physiological state. In subjects where the spatial filter would extract an inverted source signal, for instance due to EEG cap positioning, this functional relationship would be inverted, with higher response at peak states compared to trough states. Therefore, it is important to be able to uniquely define positive and negative peaks of an ongoing rhythm, which is possible when considering measures such as  $\Delta CT$ . Additionally, the concept of a protophase [27] may aid in describing non-uniform phase velocity and the resulting relationships between cognitive functions and the evolution of oscillations. In fact, as indicated in previous studies [55] duty cycle in neuronal oscillations relates to windows of opportunity for spike transfer between distinct neuronal populations. While 50% duty cycle relates to the same duration of excitatory and inhibitory phases, a deviation from this number (e.g. 30%) can introduce significantly shorter duration of excitatory phase thus providing more precise tuning for the neuronal communication, effectively blocking effects of spikes arriving at the considerably longer inhibitory phase. Spatial mixing in EEG/MEG, leading to more sinusoidal signals, might create an illusion of oscillations with 50% duty cycles while at the source level the duty cycle can be considerably different. When using band-pass filtering non-sinusoidality is removed since only one Fourier component is preserved effectively representing only one frequency and its immediate neighborhood. Behavioral and stimulation effects of such band-pass filtered signal will still be present yet neurophysiological interpretation can be different.

It has been debated whether  $\alpha/\beta$ -rhythms have a common or separate origin [29, 38, 56]. One of the arguments in favor of both rhythms originating from the same source is that if

$\alpha$ - and  $\beta$ -oscillations are generated by the same neuronal source, producing rhythmic but non-sinusoidal waveform, then one should observe a strong positive amplitude correlation between the two oscillations [38]. This argumentation is based on the linearity of the Fourier transform, as briefly illustrated in the following:

As shown above, our non-sinusoidal signal can be represented as  $S = \alpha + b \cdot \beta$ , with the corresponding Fourier transform of  $S$  being  $F(S)$ . When the amplitude of  $S$  is changing in different time segments (multiplied by  $A_i$ ), the corresponding Fourier transform at segment  $i$ , can be written as:  $F(A_i \cdot (\alpha + b \cdot \beta)) = A_i(F(\alpha)) + A_i \cdot b(F(\beta))$ , which in turns shows that the amplitude of  $\alpha$ - and  $\beta$ -oscillations should covary linearly when the amplitude of  $S$  changes by  $A_i$ . The amplitude of oscillations in different frequency bands can covary for different neuronal sources, but the presence of strong correlations between oscillations at different frequencies with similar spatial topographies is consistent with the idea of them originating from the same neuronal source. Yet, our simulations show that even when a comodulation between  $\alpha$ - and  $\beta$ -oscillations is certainly known to originate from the non-sinusoidal waveform of oscillations, due to the peculiarities of the spatial mixing, it is possible not to observe such positive comodulation. Moreover, surprisingly it is even possible to detect anticorrelation between the amplitudes of  $\alpha$ - and  $\beta$ -oscillations. However, this is entirely due to the effects of spatial mixing of individual signals each of which by itself has only positive correlations between  $\alpha$ - and  $\beta$ -oscillations. Yet, a spatial summation may lead to the occurrence of negative correlations at the sensor level. Importantly, even when using sophisticated spatial filtering techniques such as ICA, SSD, etc. it is unlikely to disentangle such spatial mixing effects originating from the local cortical patches since the resolution of EEG/MEG and even LFP recordings is not sufficient. This also applies to the argument supporting a separate origin of oscillatory components requiring independence of the corresponding temporal dynamics. We have shown that seemingly separate amplitude time courses may not be an indication for the independence of the rhythms, but can also occur when the coupling between different sources changes in the span of only a few hundreds of milliseconds. Whether  $\beta$ -events can arise through decoupling of oscillators as in the presented simulations, is a topic for further research. This can reveal insights about mesoscopic brain organization and the interplay of different local rhythms, as extracted by EEG/MEG.

Regarding cross-frequency interactions, our study shows that the amplitude-to-amplitude cross-frequency coupling can also be affected by the non-sinusoidal waveform of the oscillations. For all three types of cross-frequency interactions (phase-to-phase, phase-to-amplitude, amplitude-to-amplitude), spatial synchronization can lead to either very strong or weak indices characterizing cross-frequency interactions, corresponding respectively to a small or rather large jitter in the time delays between neuronal sources (see Fig 10). This again requires careful interpretation of the obtained data and discussion about the possible effects of spatial synchronization among neuronal populations generating EEG/MEG/LFP signals.

## Supporting information

**S1 Fig. Illustration: 1/f-corrected power spectra for different SNR-levels.** All example power spectra were computed on Laplacian-filtered C3-signals. The spectra show a clear presence of peaks in the frequency band of interest, thus justifying the selection of these subjects for further analysis. The SNR-threshold for inclusion was 5 dB.  
(TIFF)

**S2 Fig. Illustration: Asymmetric occipital  $\alpha$ -oscillations.** Each row corresponds to one SSD component extracted for different subjects. From left to right column: (1) Occipital topography. (2)  $\Delta$ CT distributions. For every oscillatory cycle, there are corresponding  $T_c$ - and  $T_r$ -

values. Red dot indicates mean  $T_c$ - and  $T_t$ -values. (3) Power spectrum showing pronounced  $\alpha$ - and  $\beta$ -peaks. Pink lines indicate  $\alpha$ -peak and first and second harmonic frequency. (4) Example time course excerpt of the SSD component.

(TIFF)

**S3 Fig. Illustration:  $\Delta CT$  for different noise levels.** The spread of  $T_c$ - and  $T_t$ -values increases with increasing noise level. Illustration was created by adding an increasing amount of  $1/f$ -noise to a oscillatory component as extracted by SSD.

(TIFF)

## Acknowledgments

We thank Elena Cesnaite and Keyvan Mahjoory for data preparation.

## Author Contributions

**Conceptualization:** Natalie Schaworonkow, Vadim V. Nikulin.

**Data curation:** Natalie Schaworonkow.

**Formal analysis:** Natalie Schaworonkow.

**Funding acquisition:** Natalie Schaworonkow, Vadim V. Nikulin.

**Investigation:** Natalie Schaworonkow, Vadim V. Nikulin.

**Methodology:** Natalie Schaworonkow, Vadim V. Nikulin.

**Project administration:** Vadim V. Nikulin.

**Resources:** Natalie Schaworonkow, Vadim V. Nikulin.

**Software:** Natalie Schaworonkow.

**Supervision:** Vadim V. Nikulin.

**Validation:** Natalie Schaworonkow.

**Visualization:** Natalie Schaworonkow.

**Writing – original draft:** Natalie Schaworonkow, Vadim V. Nikulin.

**Writing – review & editing:** Natalie Schaworonkow, Vadim V. Nikulin.

## References

1. Engel AK, Fries P. Beta-band oscillations-signalling the status quo? *Current Opinion in Neurobiology*. 2010; 20(2):156–165. <https://doi.org/10.1016/j.conb.2010.02.015> PMID: 20359884
2. Arnal LH, Giraud AL. Cortical oscillations and sensory predictions. *Trends in Cognitive Sciences*. 2012; 16(7):390–398. <https://doi.org/10.1016/j.tics.2012.05.003> PMID: 22682813
3. Brittain JS, Brown P. Oscillations and the basal ganglia: Motor control and beyond. *Neuroimage*. 2014; 85:637–647. <https://doi.org/10.1016/j.neuroimage.2013.05.084> PMID: 23711535
4. Murthy VN, Fetz EE. Coherent 25- to 35-Hz oscillations in the sensorimotor cortex of awake behaving monkeys. *Proceedings of the National Academy of Sciences*. 1992; 89(12):5670–5674. <https://doi.org/10.1073/pnas.89.12.5670>
5. Ward LM. Synchronous neural oscillations and cognitive processes. *Trends in Cognitive Sciences*. 2003; 7(12):553–559. <https://doi.org/10.1016/j.tics.2003.10.012> PMID: 14643372
6. Klimesch W. Alpha-band oscillations, attention, and controlled access to stored information. *Trends in Cognitive Sciences*. 2012; 16(12):606–617. <https://doi.org/10.1016/j.tics.2012.10.007> PMID: 23141428

7. Gross J. Analytical methods and experimental approaches for electrophysiological studies of brain oscillations. *Journal of Neuroscience Methods*. 2014; 228:57–66. <https://doi.org/10.1016/j.jneumeth.2014.03.007> PMID: 24675051
8. Jasper H. Charting the sea of brain waves. *Science*. 1948; 108(2805):343–347. <https://doi.org/10.1126/science.108.2805.343> PMID: 17810990
9. Rosenblum M, Pikovsky a, Kurths J, Schafer C, Tass Pa. Phase synchronization: from theory to data analysis. *Handbook of Biological Physics*. 2003; 4(August 2001):279–321.
10. Myrhaug D, Kjeldsen SP. Steepness and asymmetry of extreme waves and the highest waves in deep water. *Ocean Engineering*. 1986; 13(6):549–568. [https://doi.org/10.1016/0029-8018\(86\)90039-9](https://doi.org/10.1016/0029-8018(86)90039-9)
11. Brodtkorb PA, Johannesson P, Lindgren G, Rychlik I, Ryden J, Sjö E. WAFO—A Matlab Toolbox for Analysis of Random Waves and Loads. In: Tenth International Offshore and Polar Engineering Conference; 2000. p. 1–8.
12. Cole S, Voytek B. Brain oscillations and the importance of waveform shape. *Trends in Cognitive Sciences*. 2017; 21(2):137–149. <https://doi.org/10.1016/j.tics.2016.12.008> PMID: 28063662
13. Kandel A, Buzsáki G. Cellular-synaptic generation of sleep spindles, spike-and-wave discharges, and evoked thalamocortical responses in the neocortex of the rat. *Journal of Neuroscience*. 1997; 17(17):6783–6797. <https://doi.org/10.1523/JNEUROSCI.17-17-06783.1997> PMID: 9254689
14. Steriade M, Contreras D, Amzica F, Timofeev I. Synchronization of fast (30–40 Hz) spontaneous oscillations in intrathalamic and thalamocortical networks. *Journal of Neuroscience*. 1996; 16(8):2788–2808. <https://doi.org/10.1523/JNEUROSCI.16-08-02788.1996> PMID: 8786454
15. Cole SR, Voytek B. Cycle-by-cycle analysis of neural oscillations. *bioRxiv*. 2018;.
16. Dupré La Tour T, Moreau T, Jas M, Gramfort A. Multivariate Convolutional Sparse Coding for Electromagnetic Brain Signals. *Proceeding conference on neural information processing systems (NIPS)*. 2018.
17. Haegens S, Cousijn H, Wallis G, Harrison PJ, Nobre AC. Inter- and intra-individual variability in alpha peak frequency. *Neuroimage*. 2014; 92:46–55. <https://doi.org/10.1016/j.neuroimage.2014.01.049> PMID: 24508648
18. Carlqvist H, Nikulin VV, Strömberg JO, Brismar T. Amplitude and phase relationship between alpha and beta oscillations in the human electroencephalogram. *Medical and Biological Engineering and Computing*. 2005; 43(5):599–607. <https://doi.org/10.1007/BF02351033> PMID: 16411632
19. Gaarder K, Speck LB. The quasi-harmonic relations of alpha and beta peaks in the power spectrum. *Brain Research*. 1967; 4(1):110–112. [https://doi.org/10.1016/0006-8993\(67\)90155-2](https://doi.org/10.1016/0006-8993(67)90155-2) PMID: 6029942
20. Palva S, Palva JM. Discovering oscillatory interaction networks with M/EEG: challenges and breakthroughs. *Trends in Cognitive Sciences*. 2012; 16(4):219–230. <https://doi.org/10.1016/j.tics.2012.02.004> PMID: 22440830
21. Jensen O, Spaak E, Park H. Discriminating Valid from Spurious Indices of Phase-Amplitude Coupling. *eNeuro*. 2016; 3(6):ENEURO.0334–16.2016. <https://doi.org/10.1523/ENEURO.0334-16.2016> PMID: 28101528
22. Scheffer-Teixeira R, Tort AB. On cross-frequency phase-phase coupling between theta and gamma oscillations in the hippocampus. *Elife*. 2016; 5:e20515. <https://doi.org/10.7554/eLife.20515> PMID: 27925581
23. Hyafil A. Misidentifications of specific forms of cross-frequency coupling: Three warnings. *Frontiers in Neuroscience*. 2015; 9(OCT):1–6.
24. VanRullen R, Busch NA, Drewes J, Dubois J. Ongoing EEG phase as a trial-by-trial predictor of perceptual and attentional variability. *Frontiers in Psychology*. 2011; 2(APR):1–9.
25. Jensen O, Mazaheri A. Shaping Functional Architecture by Oscillatory Alpha Activity: Gating by Inhibition. *Frontiers in Human Neuroscience*. 2010; 4(November):1–8.
26. Fries P. A mechanism for cognitive dynamics: Neuronal communication through neuronal coherence. *Trends in Cognitive Sciences*. 2005; 9(10):474–480. <https://doi.org/10.1016/j.tics.2005.08.011> PMID: 16150631
27. Kralemann B, Cimponeriu L, Rosenblum M, Pikovsky A, Mrowka R. Phase dynamics of coupled oscillators reconstructed from data. *Physical Review E—Statistical, Nonlinear, and Soft Matter Physics*. 2008; 77(6):1–16.
28. Babayan A, Erbey M, Kumral D, Reinelt JD, Reiter AMF, Röbbing J, et al. Data descriptor: A mind-brain-body dataset of MRI, EEG, cognition, emotion, and peripheral physiology in young and old adults. *Scientific Data*. 2019; 6:1–21. <https://doi.org/10.1038/sdata.2018.308>
29. Nikulin VV, Brismar T. Phase synchronization between alpha and beta oscillations in the human electroencephalogram. *Neuroscience*. 2006; 137(2):647–657. <https://doi.org/10.1016/j.neuroscience.2005.10.031> PMID: 16338092

30. Blankertz B, Acqualagna L, Dähne S, Haufe S, Schultze-Kraft M, Sturm I, et al. The Berlin brain-computer interface: progress beyond communication and control. *Frontiers in Neuroscience*. 2016; 10. <https://doi.org/10.3389/fnins.2016.00530>
31. Lee T-W, Girolami M, Sejnowski TJ. Independent component analysis using an extended infomax algorithm for mixed subgaussian and supergaussian sources *Neural Computation*. 1999; 11(2):417–441. <https://doi.org/10.1162/089976699300016719> PMID: 9950738
32. Nikulin VV, Nolte G, Curio G. A novel method for reliable and fast extraction of neuronal EEG/MEG oscillations on the basis of spatio-spectral decomposition. *Neuroimage*. 2011; 55(4):1528–1535. <https://doi.org/10.1016/j.neuroimage.2011.01.057> PMID: 21276858
33. Pfurtscheller G, Neuper C, Andrew C, Edlinger G Foot and hand area mu rhythms *International Journal of Psychophysiology*. 1997; 26(1-3):121–135. [https://doi.org/10.1016/S0167-8760\(97\)00760-5](https://doi.org/10.1016/S0167-8760(97)00760-5) PMID: 9202999
34. Arroyo S, Lesser RP, Gordon B, Uematsu S, Jackson D, Webber R Functional significance of the mu rhythm of human cortex: an electrophysiologic study with subdural electrodes. *Electroencephalography Clinical Neurophysiology*. 1993; 87(3):76–87. [https://doi.org/10.1016/0013-4694\(93\)90114-B](https://doi.org/10.1016/0013-4694(93)90114-B) PMID: 7691544
35. Niedermeyer E, da Silva FL (Eds.) *Electroencephalography: basic principles, clinical applications, and related fields*. Lippincott Williams & Wilkins. 2005.
36. Spitzer B, Haegens S Beyond the status quo: A role for beta oscillations in endogenous content (re) activation. *eNeuro*. 2017; 4(4):e0170–17.2017 1–15. <https://doi.org/10.1523/ENEURO.0170-17.2017>
37. Sherman MA, Lee S, Law R, Haegens S, Thorn CA, Hämäläinen MS, Moore CI, Jones SR, Neural mechanisms of transient neocortical beta rhythms: Converging evidence from humans, computational modeling, monkeys, and mice. *Proceedings of the National Academy of Sciences*. 2016; 113(33): E4885–94. <https://doi.org/10.1073/pnas.1604135113>
38. Palva JM, Palva S, Kaila K. Phase synchrony among neuronal oscillations in the human cortex. *Journal of Neuroscience*. 2005; 25:3962–3972. <https://doi.org/10.1523/JNEUROSCI.4250-04.2005> PMID: 15829648
39. Putman P, Verkuil B, Arias-Garcia E, Pantazi I, Van Schie C. EEG theta/beta ratio as a potential biomarker for attentional control and resilience against deleterious effects of stress on attention. *Cognitive Affective Behavioral Neuroscience*. 2014; 14:782–791. <https://doi.org/10.3758/s13415-013-0238-7>
40. Clarke AR, Barry RJ, Karamacoska D, Johnstone SJ. The EEG Theta/Beta Ratio: A marker of Arousal or Cognitive Processing Capacity? *Applied Psychophysiology Biofeedback*. 2019;1–7.
41. Pfurtscheller G, Lopes da Silva FH. Event-related EEG/MEG synchronization and desynchronization: basic principles. *Clinical Neurophysiology*. 1999; 110(11):1842–1857. [https://doi.org/10.1016/S1388-2457\(99\)00141-8](https://doi.org/10.1016/S1388-2457(99)00141-8) PMID: 10576479
42. Bullock TH, McClune MC, Achimowicz JZ, Iragui-Madoz VJ, Duckrow RB, Spencer SS. EEG coherence has structure in the millimeter domain: subdural and hippocampal recordings from epileptic patients. *Electroencephalography and Clinical Neurophysiology*. 1995; 95(3):161–177. [https://doi.org/10.1016/0013-4694\(95\)93347-A](https://doi.org/10.1016/0013-4694(95)93347-A) PMID: 7555907
43. Hohlefeld F, Huchzermeyer C, Huebl J, Schneider GH, Brücke C, Schönecker T, et al. Interhemispheric functional interactions between the subthalamic nuclei of patients with Parkinson's disease. *European Journal of Neuroscience*. 2014; 40(8):3273–3283. <https://doi.org/10.1111/ejn.12686> PMID: 25195608
44. Maris E, Womelsdorf T, Desimone R, Fries P. Rhythmic neuronal synchronization in visual cortex entails spatial phase relation diversity that is modulated by stimulation and attention. *Neuroimage*. 2013; 74:99–116. <https://doi.org/10.1016/j.neuroimage.2013.02.007> PMID: 23416733
45. Krusienski DJ, Schalk G, McFarland DJ, Wolpaw JR. A  $\mu$ -rhythm matched filter for continuous control of a brain-computer interface. *IEEE Transactions on Biomedical Engineering*. 2007; 54(2).273–280. <https://doi.org/10.1109/TBME.2006.886661> PMID: 17278584
46. Brunner C, Allison BZ, Krusienski DJ, Kaiser V, Müller-Putz GR, Pfurtscheller G, Neuper C. Improved signal processing approaches in an offline simulation of a hybrid brain-computer interface. *Journal of Neuroscience Methods* 2010; 188(1):165–173. <https://doi.org/10.1016/j.jneumeth.2010.02.002> PMID: 20153371
47. Lozano-Soldevilla D, ter Huurne N, Oostenveld R. Neuronal Oscillations with Non-sinusoidal Morphology Produce Spurious Phase-to-Amplitude Coupling and Directionality. *Frontiers in Computational Neuroscience*. 2016; 10:1–17. <https://doi.org/10.3389/fncom.2016.00087>
48. Jansen BH, Rit VG. Electroencephalogram and visual evoked potential generation in a mathematical model of coupled cortical columns. *Biological Cybernetics*. 1995; 73:357–366. <https://doi.org/10.1007/BF00199471> PMID: 7578475

49. Wendling F, Bartolomei F, Bellanger JJ, Chauvel P. Epileptic fast activity can be explained by a model of impaired GABAergic dendritic inhibition. *European Journal of Neuroscience*. 2002; 15:1499–1508. <https://doi.org/10.1046/j.1460-9568.2002.01985.x> PMID: 12028360
50. Jones SR, Pritchett DL, Sikora MA, Stufflebeam SM, Hämäläinen MS, Moore CI. Quantitative analysis and biophysically realistic neural modeling of the MEG mu rhythm: rhythmogenesis and modulation of sensory-evoked responses. *Journal of Neurophysiology*. 2009; 102:3554–3572. <https://doi.org/10.1152/jn.00535.2009> PMID: 19812290
51. Shahbazi Avarvand F, Bartz S, Andreou C, Samek W, Leicht G., Mulert C., et al. Localizing bicoherence from EEG and MEG. *NeuroImage* 2018; 174:352–363. <https://doi.org/10.1016/j.neuroimage.2018.01.044> PMID: 29421325
52. Bartz S, Avarvand FS, Leicht G, Nolte G. Analyzing the waveshape of brain oscillations with bicoherence. *NeuroImage*. 2019; 188: 145–160. <https://doi.org/10.1016/j.neuroimage.2018.11.045> PMID: 30502446
53. Zrenner C, Desideri D, Belardinelli P, Ziemann U. Real-time EEG-defined excitability states determine efficacy of TMS-induced plasticity in human motor cortex. *Brain Stimulation*. 2018; 11(2):374–389. <https://doi.org/10.1016/j.brs.2017.11.016> PMID: 29191438
54. Hanslmayr S, Volberg G, Wimber M, Dalal SS, Greenlee MW. Prestimulus oscillatory phase at 7 Hz gates cortical information flow and visual perception. *Current Biology*. 2013; 23(22):2273–8. <https://doi.org/10.1016/j.cub.2013.09.020> PMID: 24184106
55. Buzsáki G, Draguhn A, Draguhn A. Neuronal oscillations in cortical networks. *Science*. 2004; 304(5679):1926–1929. <https://doi.org/10.1126/science.1099745> PMID: 15218136
56. Hari R, Salmelin R. Human cortical oscillations: A neuromagnetic view through the skull. *Trends in Neurosciences*. 1997; 20(1):44–49. [https://doi.org/10.1016/S0166-2236\(96\)10065-5](https://doi.org/10.1016/S0166-2236(96)10065-5) PMID: 9004419